NASA Technical Paper 1142

Evaluation of a Laboratory Test Model Annular Momentum Control Device

Nelson J. Groom and David E. Terray

MARCH 1978

NASA

NASA Technical Paper 1142

Evaluation of a Laboratory Test Model Annular Momentum Control Device

Nelson J. Groom and David E. Terray
Langley Research Center
Hampton, Virginia

National Aeronautics
and Space Administration

**Scientific and Technical
Information Office**

1978

SUMMARY

A 4068 N-m-sec (3000 lb-ft-sec) laboratory test model annular momentum control device (AMCD) is described and static and dynamic test results are presented. An AMCD is a spinning annular rim suspended by noncontacting magnetic bearings and powered by a noncontacting linear electromagnetic motor. Test results include spin-motor torque characteristics and spin-motor and magnetic-bearing drag losses. Limitations of some of the design approaches taken are also discussed.

INTRODUCTION

The annular momentum control device (AMCD) represents a new development in the field of momentum storage devices (ref. 1). The basic concept of the AMCD is that of a rotating annular rim suspended by noncontacting magnetic bearings and powered by a noncontacting linear electromagnetic motor (fig. 1). A detailed discussion of the rationale for the AMCD configuration and its potential applications are presented in reference 2. Although the majority of the applications discussed in the reference are spacecraft oriented, it appears that the concept may also have significant advantages as an energy storage device for Earth-based applications (refs. 3 to 5). Because of its unique configuration, an AMCD presents several design constraints which interact with all components and result in basic requirements for any AMCD design. As pointed out in reference 2, any number of variations in the design of rim, motor, and/or bearings could be made in an attempt to better meet the specific design requirements for a given application. General design considerations are listed and discussed in this reference. In order to investigate any potential problem areas in implementing the AMCD concept for large radial dimensions, a laboratory test model AMCD was designed and fabricated under contract. The laboratory model has been delivered and preliminary tests performed. This paper includes a brief description of the laboratory model AMCD assembly and results of static and low-speed dynamic tests.

SYMBOLS

K_A	position gain
K_B	electromagnet gain
K_m	equivalent permanent-magnet stiffness
K_R	derived rate gain
m	suspended mass
P	power
s	Laplace variable

x	rim displacement
x_c	position command
ω	frequency

MODEL DESCRIPTION

A brief description of the laboratory model AMCD shown in figure 2 is presented in this section. A more detailed description of the subsystems is given in reference 6. The laboratory model (fig. 2) consists of a graphite-epoxy composite rim which is 1.6 m (63 in.) in diameter, weighs 22.4 kg (49.4 lb), and is designed to rotate at a speed of 2703 rpm. At this speed the rim momentum is 4068 N-m-sec (3000 lb-ft-sec). The rim is suspended by three equally spaced suspension stations. Magnetic-bearing elements located in the suspension stations interact with a low-loss ferrite material, embedded in the rim, to produce radial and axial suspension forces. Electromagnetic stator elements, also located at the suspension stations, push and pull against 72 equally spaced samarium cobalt permanent magnets, embedded in the rim near the outer edge, to produce spin torques. The stator-element drive electronics are commutated by signals from a Hall effect device which senses the position of the magnets.

In order to prevent damage to the rim in the event of a magnetic suspension failure during spin tests, the AMCD laboratory model assembly includes a backup bearing system. The system has six bearings (two per suspension station) which are designed to slow and support the rim. The bearing system provides hydrostatic air pads for radial control and hydrodynamic air pads for axial control. The backup and suspension bearing assemblies are supported by an aluminum baseplate. A vacuum cover (not shown) fits over the bearing-motor-rim assembly and bolts to the baseplate for high-speed spin tests.

Figure 3 is a close-up of one of the suspension stations. There are eight magnetic-bearing elements, four top and four bottom, which provide axial suspension. A total of four elements are mounted around the inside of the rim which, in conjunction with the other two stations, provide radial suspension. The center structure mounts the axial- and radial-position sensors for this station. The sensors consist of a variable-impedance bridge with an active coil and a reference coil. They are sensitive to anything that changes the inductance of the active coil in the sensor probe such as the close proximity of a magnetic material. In the AMCD rim the ferrite material is sensed. Figure 4 is a cross-sectional drawing of a suspension station and shows the rim, bearings, and spin-motor elements in more detail. The magnetic-bearing gaps with the rim centered are 2.54 mm (0.1 in.).

RESULTS AND DISCUSSION

Magnetic-Bearing System

As described in reference 6, the AMCD magnetic bearings utilize permanent-magnet flux biasing. The advantages of this technique include (1) a linear

relationship between force and current at a given operating point can be easily obtained, (2) with permanent magnets supplying a portion of the flux, the power required to suspend the rim in a 1g (1g = 9.8 m/sec^2 (32.2 ft/sec^2)) environment is reduced, and (3) the permanent magnets supply the constant flux required for zero-power operation.

The force produced by a given station at a given equilibrium position can be represented by the following equation from reference 6:

$$F = K_B I + K_m x \tag{1}$$

where K_B is the electromagnet gain in force units per unit current, K_m is an equivalent permanent-magnet stiffness in force units per unit displacement, I is a given electromagnet current, and x is a given rim displacement. A simplified block diagram of a magnetic-bearing suspension servo using the force model of equation (1) is shown in figure 5 where K_A is the position gain, K_R is the derived rate gain, and m is the suspended mass. The closed-loop transfer function becomes

$$\frac{x}{x_c} = \frac{K_A K_B/m}{s^2 + \left(\frac{K_R K_B}{m}\right)s + \left(\frac{K_A K_B - K_m}{m}\right)} \tag{2}$$

which is a classical second-order transfer function with a natural frequency of

$$\omega_n = \sqrt{\frac{K_A K_B - K_m}{m}} \tag{3}$$

and a damping ratio of

$$\rho = \left(\frac{1}{2\omega_n}\right)\frac{K_R K_B}{m} \tag{4}$$

The conditions for stability are $K_A K_B > K_m$ and $K_R > 0$. The dc gain of the system becomes

$$\left.\frac{x}{x_c}\right|_{s=0} = \frac{1}{1 - \left(\frac{K_m}{K_A K_B}\right)} \tag{5}$$

From equation (5) it is obvious that as $K_A K_B \to K_m$, hence as $\omega_n \to 0$, $\left.\frac{x}{x_c}\right|_{s=0} \to \infty$. Figure 6 is a Bode plot illustrating the variation in closed-loop

gain in dB at different natural frequencies normalized to $\sqrt{K_m/m}$. As can be seen from this figure, the zero dB crossover frequency approaches $\sqrt{K_m/m}$ as a lower limit. Early tests revealed that the rim had structural modes (characteristics of the rim are described in a subsequent section) close enough to the lower bandwidth limit determined by the permanent magnets to restrict the amount of rate gain that could be utilized without causing structural ringing. Conventional methods of filtering out the structural frequencies were unsuccessful due to the extreme sensitivity of the system poles to the introduction of lags down to frequencies which included the structural frequencies of interest. Low system damping, along with other effects of permanent-magnet flux biasing, and rim warp (to be discussed subsequently) combined to prevent the rim from attaining a stable spin speed in excess of 475 rpm.

Virtually zero-power (VZP) mode.- As described in reference 6, the VZP mode consists of a method to bias the equilibrium point of the rim to a position in the bearing gaps where the mass of the rim is supported by flux supplied only by the permanent magnets. The advantage of this method is lower power consumption in a 1g environment. However, the VZP equilibrium point for the laboratory model was approximately 1.143 mm (0.045 in.) above the center of the bearing gaps. This was found to be insufficient clearance for spin tests, and since changing between VZP and position modes necessitated resetting the backup bearings, the VZP mode was not utilized beyond preliminary static tests.

Wahoo mode.- The Wahoo mode, as described in reference 6, performs a function for the radial suspension equivalent to the function performed by the VZP mode for the axial suspension with the added feature of allowing for rim expansion at higher speeds. In the laboratory model tests the assembly was mounted with the rim spin axis vertical so the equilibrium radial position was centered in the bearings. However, since the radial-position mode exhibited better damping than the Wahoo mode and the axial bearings were supporting the rim weight, the radial-position mode was utilized for the majority of the spin tests.

Rim

Rim fabrication.- The laboratory model AMCD rim was fabricated by wrapping a graphite filament tape, impregnated with resin, on a special spindle producing 100-percent circumferential fibers (ref. 6). The advantage of this technique is that the full strength of the material can be utilized (ref. 2). However, since the fibers are 100-percent circumferential, the only resistance to creep along the axis parallel to the spin axis is provided by epoxy. It was discovered early in the test program that care must be exercised in storing the rim in a 1g environment to prevent the rim from creeping. The creep is in a direction which produces deviations out of the spin plane. These deviations produce an equivalent disturbance input to the axial bearings as the rim spins. In the laboratory model AMCD, static deviations of the rim have been measured and range from a maximum of 1.651 mm (0.065 in.) to a minimum of 0.2032 mm (0.008 in.), depending on how the rim is stored. These numbers are total deviations (measured from peak to peak) and were measured midway between suspension stations with the rim suspended. The rim deviations, or warp, include two high and two low points per rim revolution, which approximates a sine wave disturbance at twice the wheel spin frequency. The origin of the basic two-cycle-per-revolution shape of the

warp is unknown. By experimenting with different methods of storing the rim, it was found that rim deviations could be held consistently to 0.381 mm (0.015 in.). This appears to be an acceptable value but confirmation awaits higher speed spin tests. Theoretically, as rim spin speed increases and rim stiffening occurs (ref. 2), the rim should flatten out and rim warp should become negligible. In the radial direction, deviations of 0.1016 mm (0.004 in.) from peak to peak were measured and exhibited a three-cycle-per-revolution shape. There was no significant change with respect to time observed for the radial deviations.

Rim structural modes.- The rim had out-of-plane bending resonances at about 18, 180, 290, 435, 610, and 800 Hz. These resonances were obtained by a frequency sweep with the rim suspended and not spinning. The resonance at 180 Hz proved to be the most severe and was the one which was excited by the bearing servo loops when an attempt was made to increase rate gain.

Drag Losses

Data for calculating drag losses were taken by spinning the rim up to 304 rpm and letting it coast down to 50 rpm. Rim warp was measured at the beginning of spin-up and at the end of spin-down and was 0.3683 mm (0.0145 in.). Pressure inside the vacuum enclosure was 11.6 Pa (87 μm Hg) at the beginning of spin-up and 14.4 Pa (108 μm Hg) at the end of spin-down. Rim speed was sampled and recorded at 5-sec intervals using the test setup described in appendix A. These data were then used to generate the rim-speed-versus-time curve shown in figure 7. The crossmarks in the plot are data points and the curve drawn through these points was generated using the curve-fit technique described in appendix B. This curve was used to calculate coefficients of a drag-loss-versus-rim-speed curve (also described in appendix B). Figure 8 is a plot of drag loss in watts as a function of rim speed in rpm over the spin-down range, and figure 9 is a similar plot over the range of 0 to 3000 rpm. The coefficients of the drag-loss equation in watts as a function of w, rim speed in rpm, were calculated to be

$$P = 7.045(10)^{-3}w + 3.057(10)^{-5}w^2 \qquad (6)$$

where the first-order term represents hysteresis loss and the second-order term represents eddy current loss. This calculation represents total drag loss, which includes losses due to the flux of the motor magnets cutting the aluminum baseplate and cover, motor-stator cores, and bearing-element cores. Total drag loss also includes losses in the rim ferrite material due to the flux from the bearing elements cutting it, losses in both the rim ferrite and bearing-element cores due to bearing-element flux change caused by gap changes introduced by rim warp, and air drag due to the residual pressure in the vacuum enclosures. An initial estimate of drag losses was made for the motor-magnet flux cutting the aluminum baseplate and cover, the magnetic-bearing flux cutting the rim ferrite, and the graphite-epoxy material of the rim. Drag loss at a pressure of 4.67 Pa (35 μm Hg) at full speed (2703 rpm) was estimated to be 1 watt. Using the same formulation for a pressure of 14.4 Pa (108 μm Hg), the drag loss becomes 3.04 watts. Total estimated drag loss from the sources just mentioned is

approximately 6 watts at full speed. The majority of the projected drag loss appears to be due to the loss caused by the motor-magnet flux cutting the motor-stator and bearing-element cores and the loss in the bearing-element cores and rim ferrite caused by rim motion resulting from rim warp. The projected drag loss (fig. 9) should be a worst-case number since high-speed effects such as rim flattening and skin effect are not accounted for.

Rim-Drive Motor

Performance data for the rim-drive motor were taken in the region from 75 to 300 rpm. Motor speed was sampled at 5-sec intervals using the test setup described in appendix A. These data were then used to generate the rim-speed-versus-time curve shown in figure 10. The crossmarks in the plot are data points and the curve drawn through them is generated by the curve-fit technique described in appendix B. The rim acceleration, calculated from figure 10, appeared to be a constant 1 rpm/sec over the range of the data. The motor torque was calculated to be 1.482 N-m (1.094 lb-ft).

CONCLUDING REMARKS

A laboratory test model AMCD has been designed and fabricated. Initial tests with the laboratory model have provided insight into limitations of some design approaches taken. These approaches are (1) permanent-magnet flux-biased magnetic bearings, (2) completely unidirectional lay-up of composite materials for the rim, and (3) possibly the use of open permanent magnets for the spin-motor poles.

Permanent-Magnet Flux Biasing

Permanent-magnet flux biasing of magnetic bearings presents advantages from the standpoint of lower power required for support in a 1g environment and linearization of current-input—force-output characteristics. This approach did, however, present a problem from a control-system standpoint for the laboratory test model AMCD. For stability, a lower limit on the servo bandwidth is imposed by the characteristics of the permanent magnets. The existence of structural modes in the area of the magnetic-bearing servo crossover of the laboratory model has limited the amount of rate gain that could be utilized without causing structural ringing. Low system damping, along with other effects of permanent-magnet flux biasing, and rim warp (to be discussed subsequently) combined to prevent the rim from attaining a stable spin speed in excess of 475 rpm. As part of the AMCD development program, work is being done on the design and fabrication of a magnetic-bearing system, with no permanent-magnet flux biasing, to replace the existing bearings.

Rim Fabrication

The rim fabrication included a unidirectional lay-up of graphite fibers, bonded by epoxy, in a circumferential direction. The advantage of this tech-

nique is that the full strength of the fibers can be utilized. However, since the fibers are 100-percent circumferential, the only resistance to creep along the axis parallel to the spin axis is provided by epoxy. Consequently, care must be exercised in storing the rim in a 1g environment to prevent the rim from creeping. The creep is in a direction which produces deviations out of the spin plane. These deviations produce an equivalent disturbance input to the axial bearings as the rim spins. Creep in the radial direction has been negligible. Problems of creep in subsequent rims could be reduced by dedicating some of the fibers to producing stiffness in the axial direction.

Spin Motor

Preliminary tests of the AMCD laboratory model indicate that the rim spin motor performs reliably and produces adequate torque. The motor produces a torque of 1.483 N-m (1.094 lb-ft) over the range (up to 300 rpm) tested. However, based on spin-down data taken over this range, the projected drag losses at rated speed are much higher than originally predicted. Most of the loss can be attributed to the flux from the open permanent-magnet motor poles cutting the motor-stator and bearing-element cores and to the loss in the bearing-element cores and rim ferrite caused by rim motion resulting from rim warp. Further tests at higher speeds will be required to confirm the projected drag losses and to separate the contributions of each source. The possibility exists that the losses due to the open permanent-magnet motor poles may be high enough to warrant reevaluation of the concept for subsequent designs.

Langley Research Center
National Aeronautics and Space Administration
Hampton, VA 23665
February 10, 1978

APPENDIX A

DATA ACQUISITION SYSTEM USED IN AMCD SPIN-UP AND SPIN-DOWN TESTS

The test setup used to obtain data during the laboratory model AMCD spin-up and spin-down tests is shown in figure 11. The setup consisted of two digital counters and a two-channel digital printer. One counter was allowed to run free under control of its internal time-base oscillator to provide time in seconds. The other counter provided a readout of rim speed by counting motor commutation pulses for one phase at a preset time interval. (For a detailed description of the spin motor see ref. 6.) At the end of this interval a print command was sent to the printer which then recorded the rim speed and time count contained in the other counter at that particular instant. The sample-rate control of the rim-speed counter was set to initiate the counting intervals every 5 sec. The preset time interval of the rim-speed counter was 1/36 min. Since there are 36 commutation pulses per phase for one revolution of the rim (ref. 6), this resulted in a direct display of revolutions per minute (rpm).

APPENDIX B

DRAG-LOSS AND MOTOR-TORQUE CALCULATIONS

This appendix presents the method used to calculate the coefficients of the drag-loss-versus-rim-speed equation based on data taken during spin-down and the equations of motor torque based on data taken during spin-up.

Drag Loss

Instantaneous torque on the rim can be expressed as

$$T = I \frac{dw}{dt} \tag{B1}$$

where T is torque, I is rim inertia, and dw/dt is the rate of change of rim speed with respect to time. The instantaneous power can be represented as

$$P = Tw \tag{B2}$$

or, by using equation (B1), as

$$P = Iw \frac{dw}{dt} \tag{B3}$$

Since I is known, only the rate of change of rim speed at a given speed is needed to compute the instantaneous drag power. Using the test setup described in appendix A, rim speed was recorded at 5-sec intervals as the rim was allowed to spin-down from 304 to 50 rpm. A curve-fit program (curve fitting by Chebyshev polynomials) was used on a desk-top calculator to generate a fourth-order curve fit through these data which resulted in a polynomial of the form

$$w = a_0 + a_1 t + a_2 t^2 + a_3 t^3 + a_4 t^4 \tag{B4}$$

Equation (B4) was then differentiated to form

$$\frac{dw}{dt} = a_1 + 2a_2 t + 3a_3 t^2 + 4a_4 t^3 \tag{B5}$$

Then w and dw/dt were computed at given values of t and equation (B3) was used to compute drag power at these specific points.

The curve-fit program was then used to fit a second-order curve through these values which resulted in a polynomial of the form

$$P = \hat{a}_1 w + \hat{a}_2 w^2 \tag{B6}$$

It should be noted that the constant term $\hat{a}_0$ was not exactly zero in equation (B6). However, it was relatively small and was ignored.

Motor Torque

Using the test setup described in appendix A, rim speed was recorded at 5-sec intervals as it was accelerated by the spin motor from 75 to 300 rpm. The data indicated constant acceleration over this range so the curve-fit program mentioned previously was used to obtain a first-order curve fit. This resulted in a polynomial of the form

$$w = \bar{a}_0 + \bar{a}_1 t \tag{B7}$$

Differentiating this equation results in

$$\frac{dw}{dt} = \bar{a}_1 \tag{B8}$$

Equation (B8) was then substituted into equation (B1) to compute the motor torque.

REFERENCES

1. Anderson, Willard W.; and Groom, Nelson J.: Annular Momentum Control Device Used for Stabilization of Space Vehicles and the Like. U.S. Patent 3,915,416, Oct. 28, 1975.

2. Anderson, Willard W.; and Groom, Nelson J.: The Annular Momentum Control Device (AMCD) and Potential Applications. NASA TN D-7866, 1975.

3. Schlieben, Ernest W.: Systems Aspects of Energy Wheels. Proceedings of the 1975 Flywheel Technology Symposium. G. C. Chang and R. G. Stone, eds., ERDA 76-85, Nov. 1975, pp. 40-52.

4. Aaland, Kristian; and Lane, Joe E.: Ideas and Experiments in Magnetic Interfacing. Proceedings of the 1975 Flywheel Technology Symposium, G. C. Chang and R. G. Stone, eds., ERDA 76-85, Nov. 1975, pp. 123-132.

5. Kirk, James A.; Studer, Philip A.; and Evans, Harold E.: Mechanical Capacitor. NASA TN D-8185, 1976.

6. Ball Brothers Research Corp.: Annular Momentum Control Device (AMCD). Volumes I and II. NASA CR-144917, [1976].

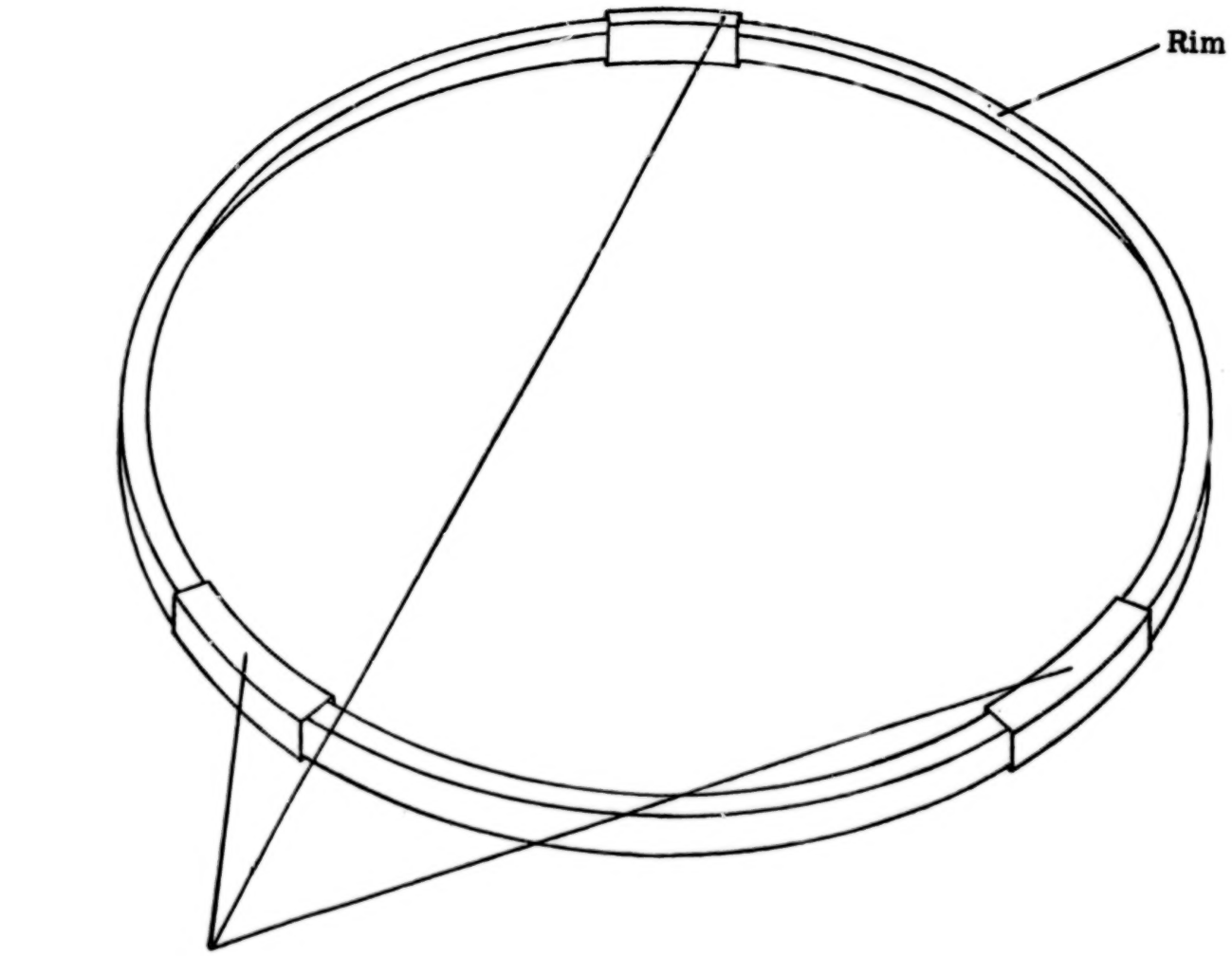

Figure 1.- Annular momentum control device concept.

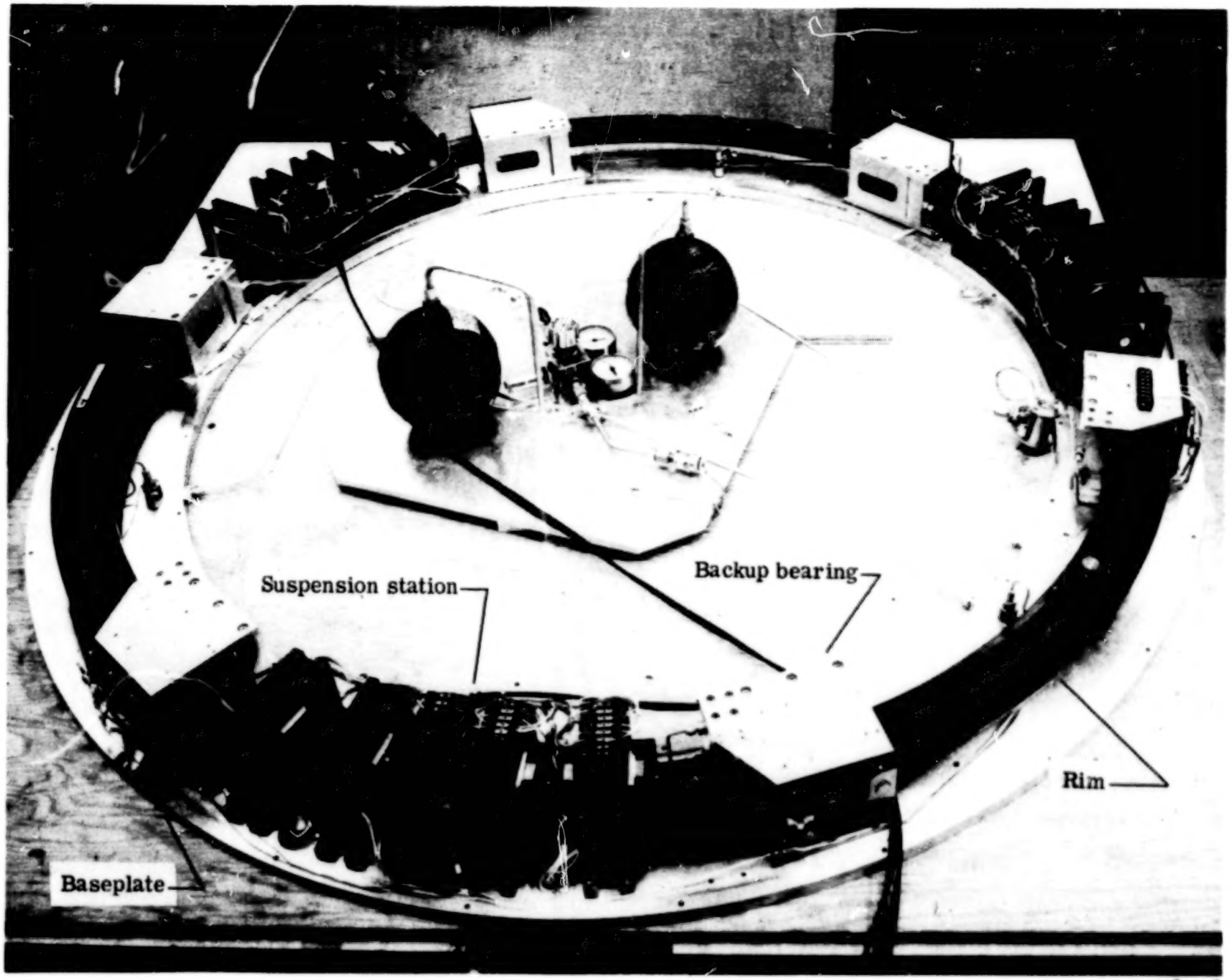

L-78-18

Figure 2.- AMCD laboratory test model.

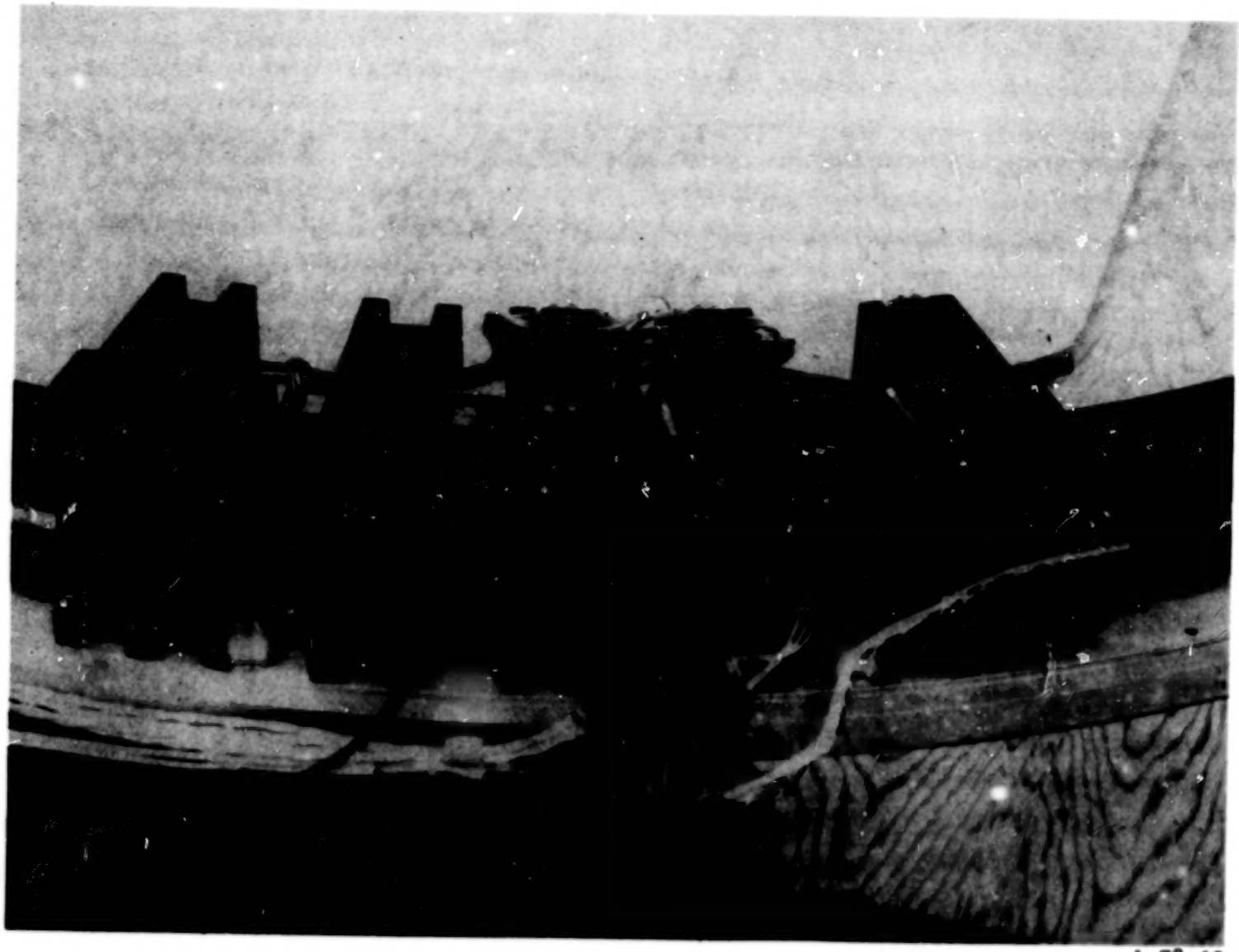

L-78-19

Figure 3.- AMCD suspension station.

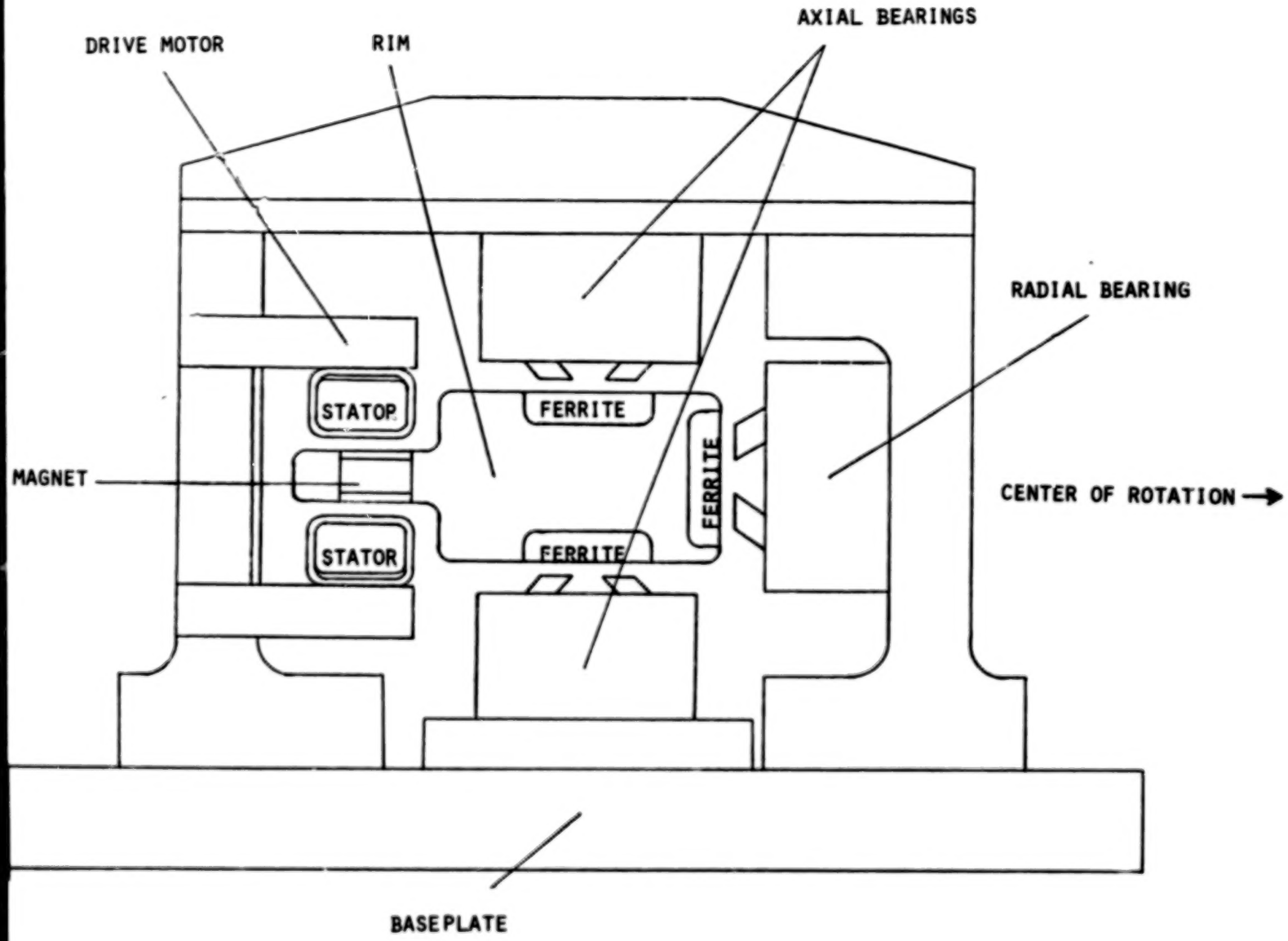

Figure 4.- Cross-section drawing of an AMCD suspension station.

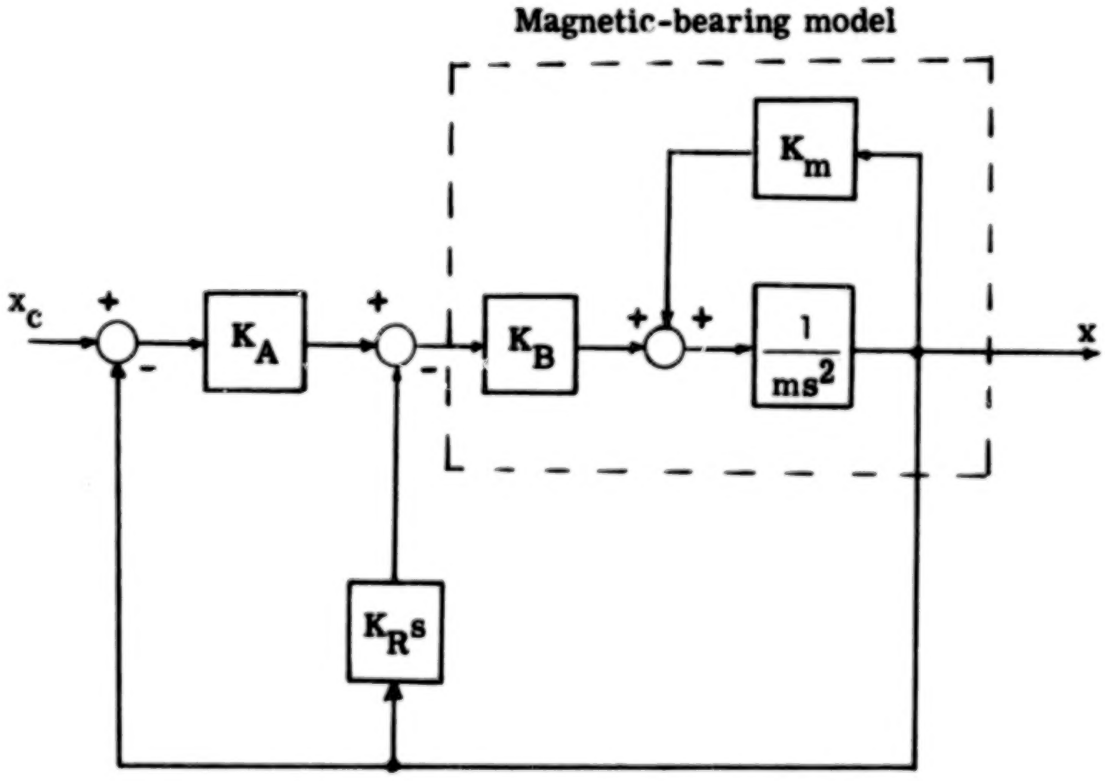

Figure 5.- Block diagram of simplified magnetic-bearing suspension servo.

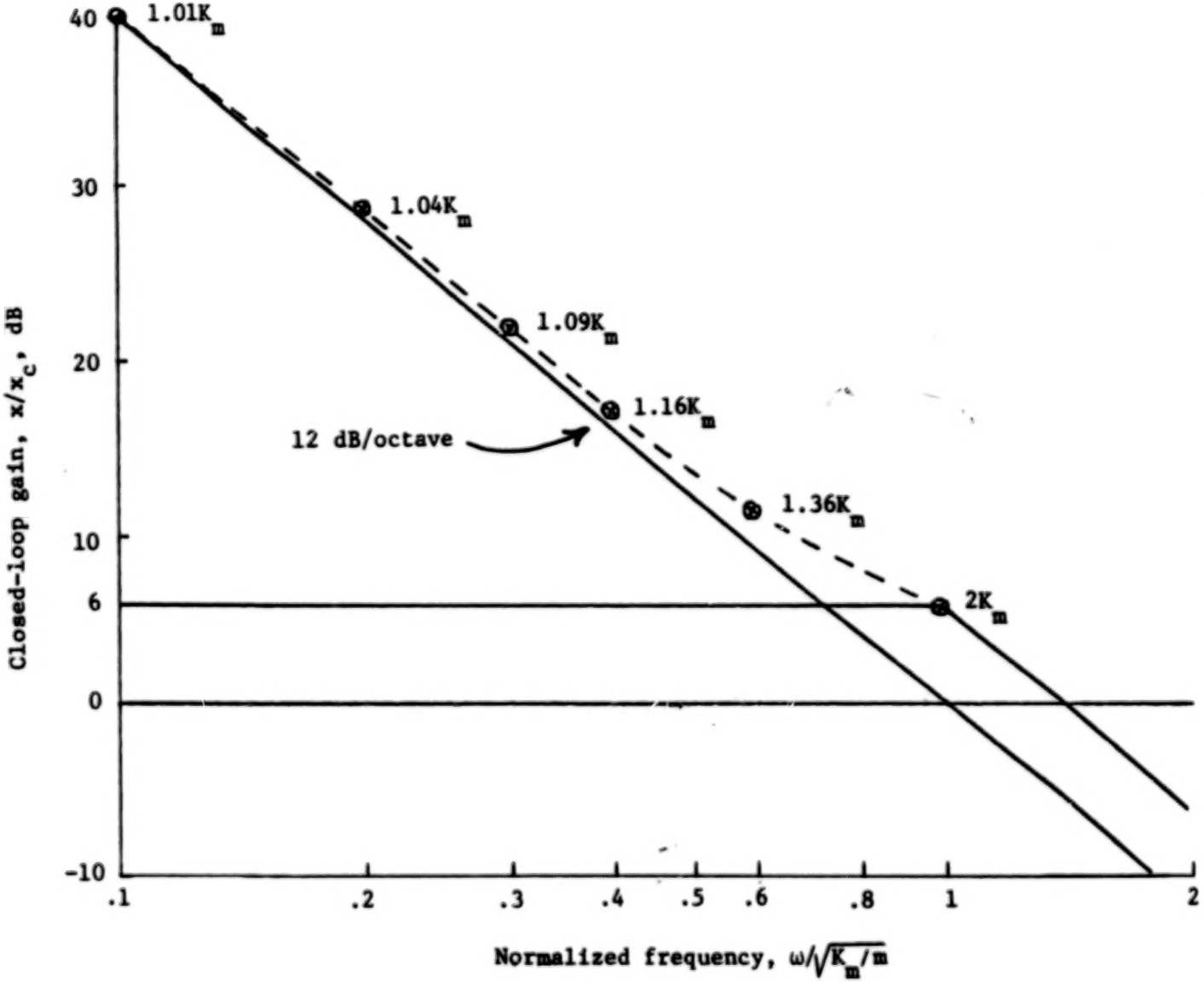

Figure 6.- Frequency-response asymptotes for simplified magnetic-bearing suspension servo with $K_A K_B$ between $1.01K_m$ and $2K_m$.

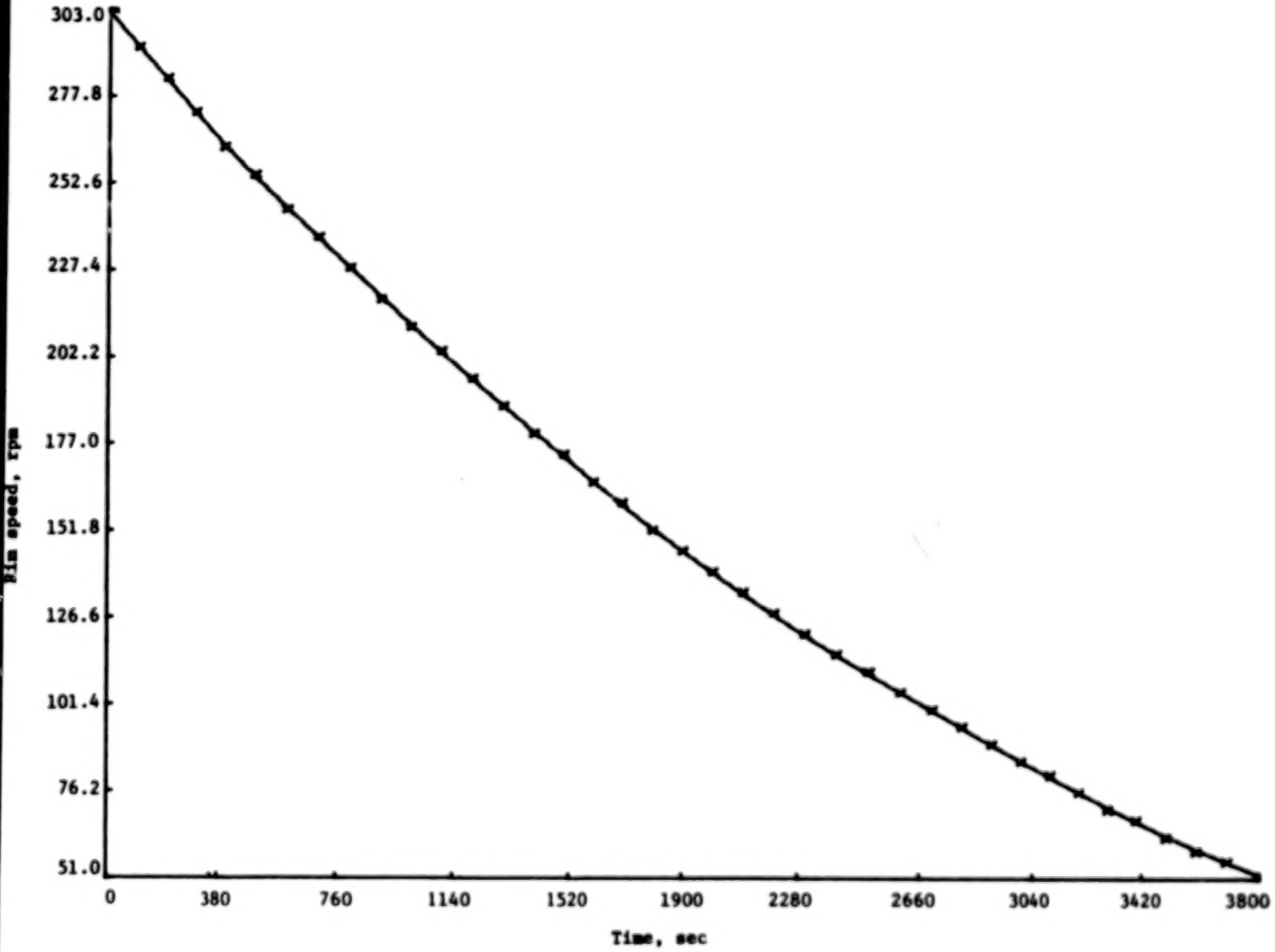

Figure 7.- Rim speed plotted against time during spin-down.

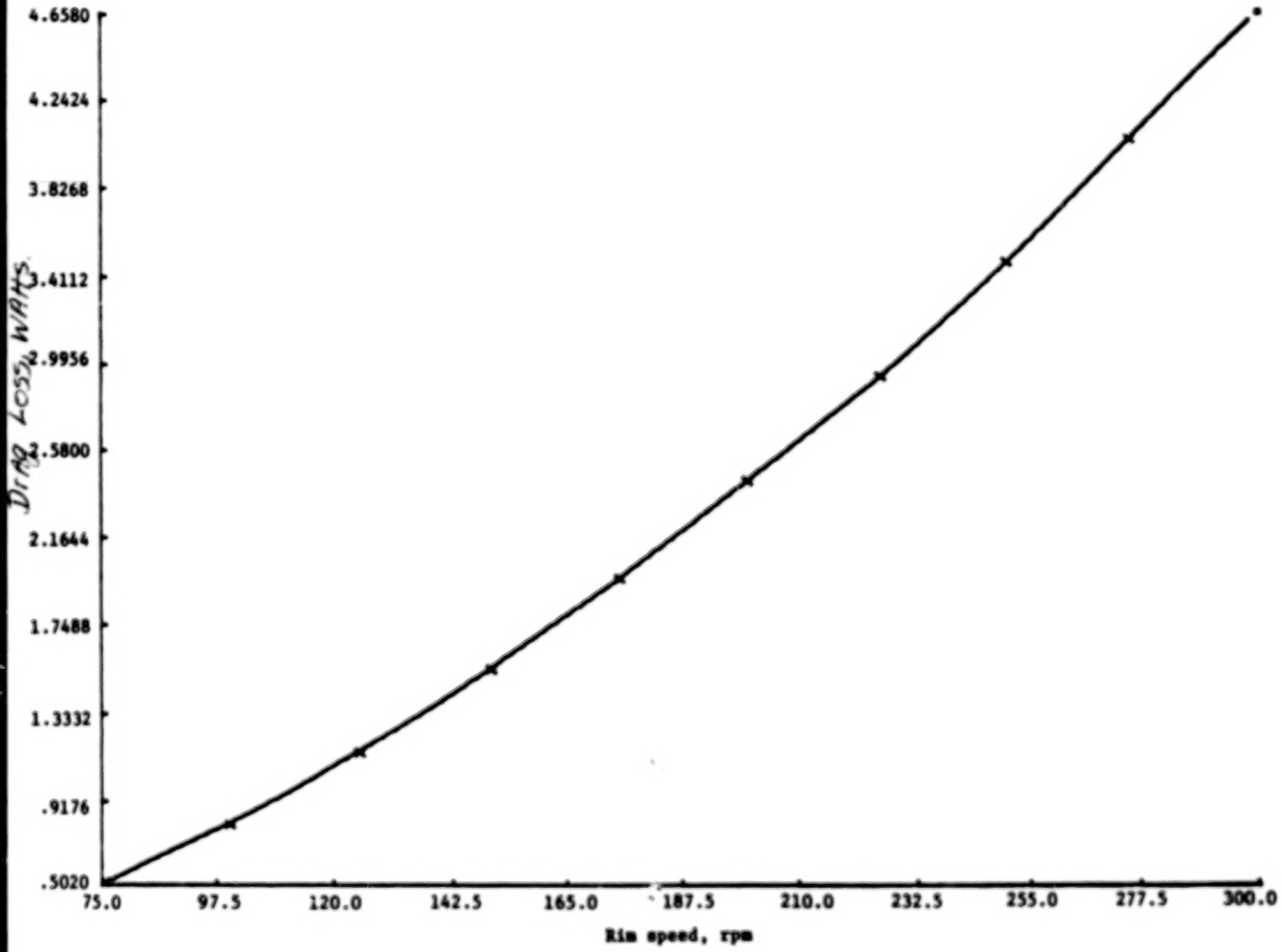

Figure 8.- Drag loss plotted against rim speed over spin-down range.

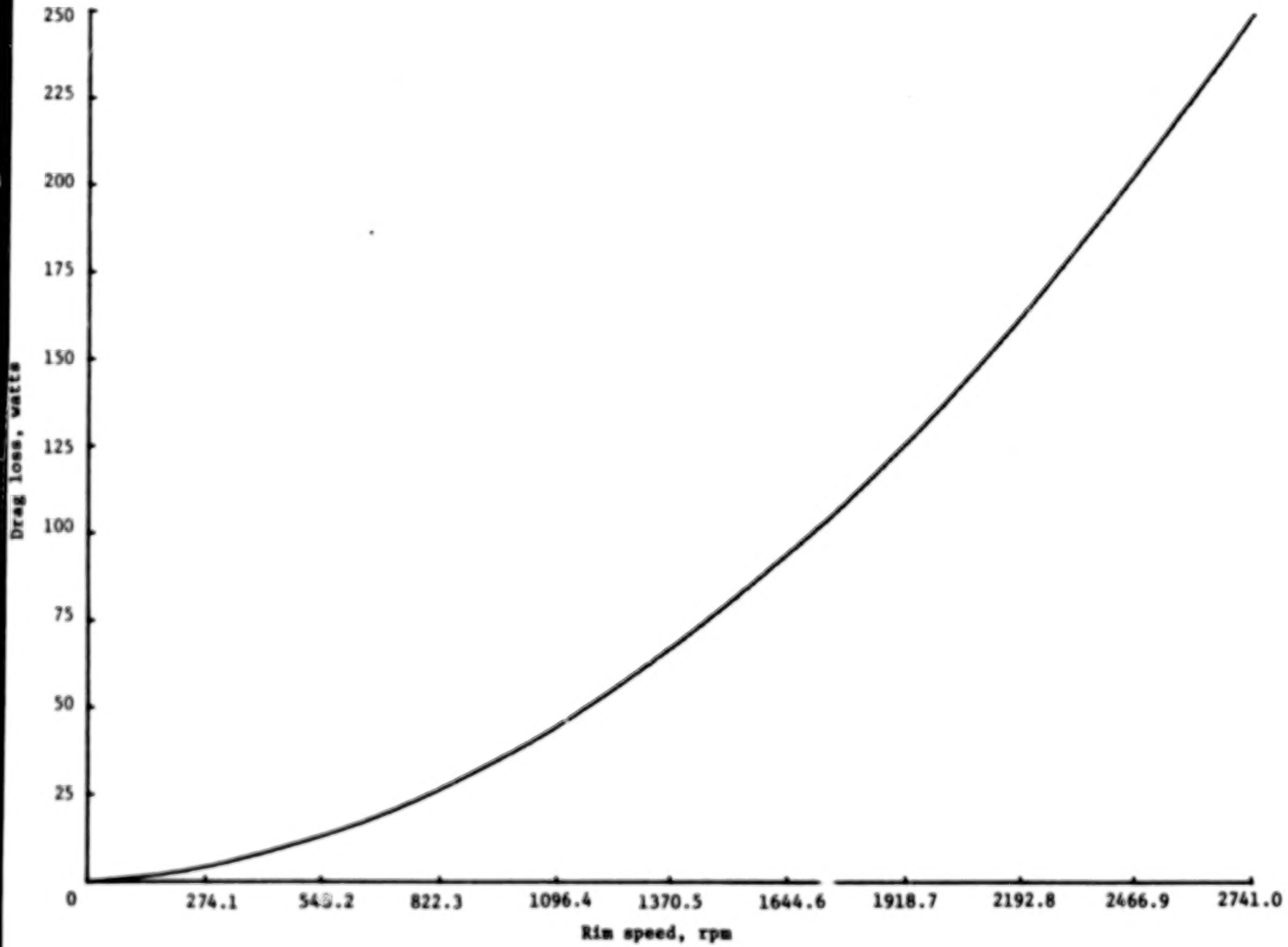

Figure 9.- Total drag loss projected to full speed.

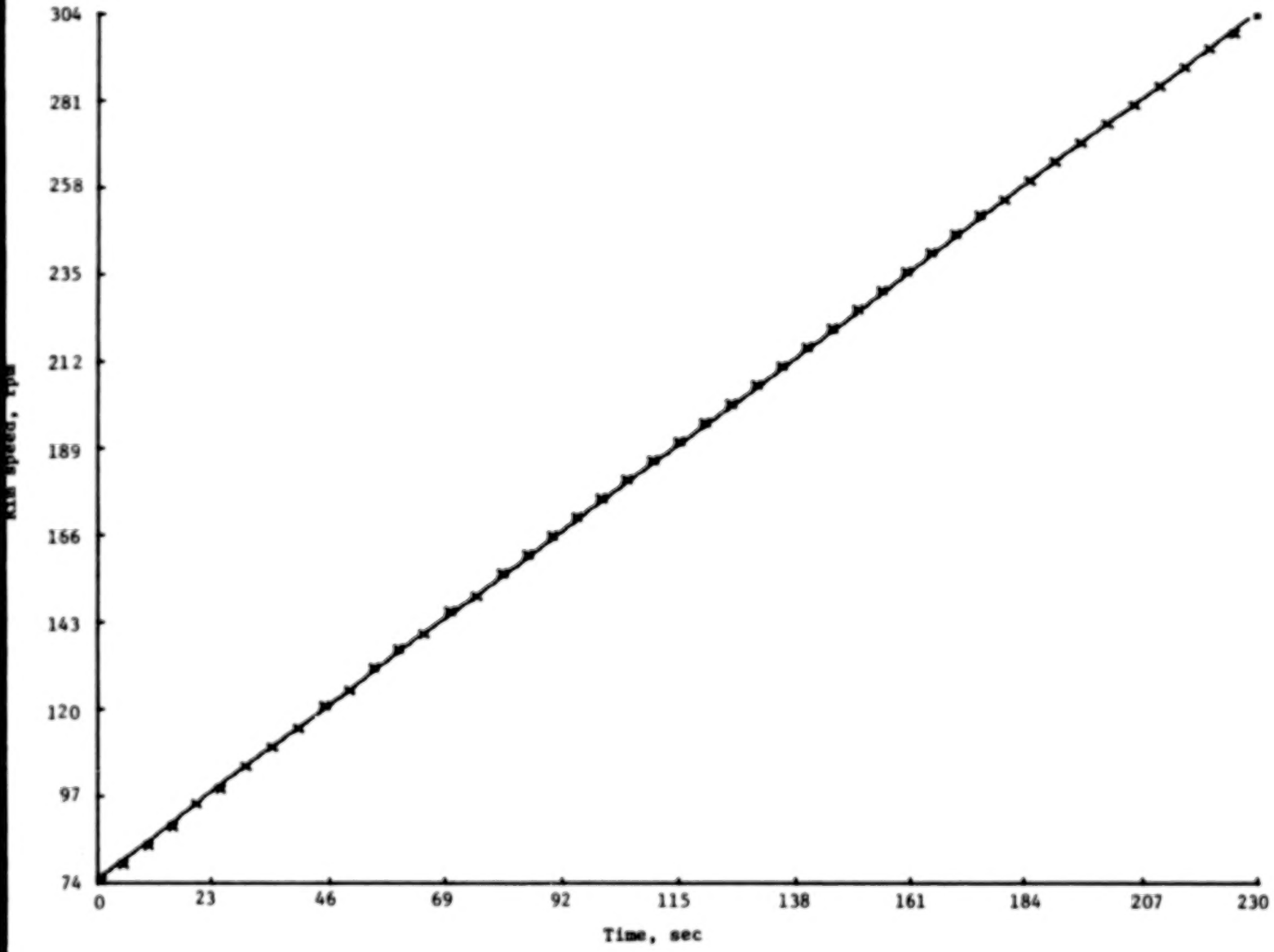

Figure 10.- Rim speed plotted against time over spin-up range.

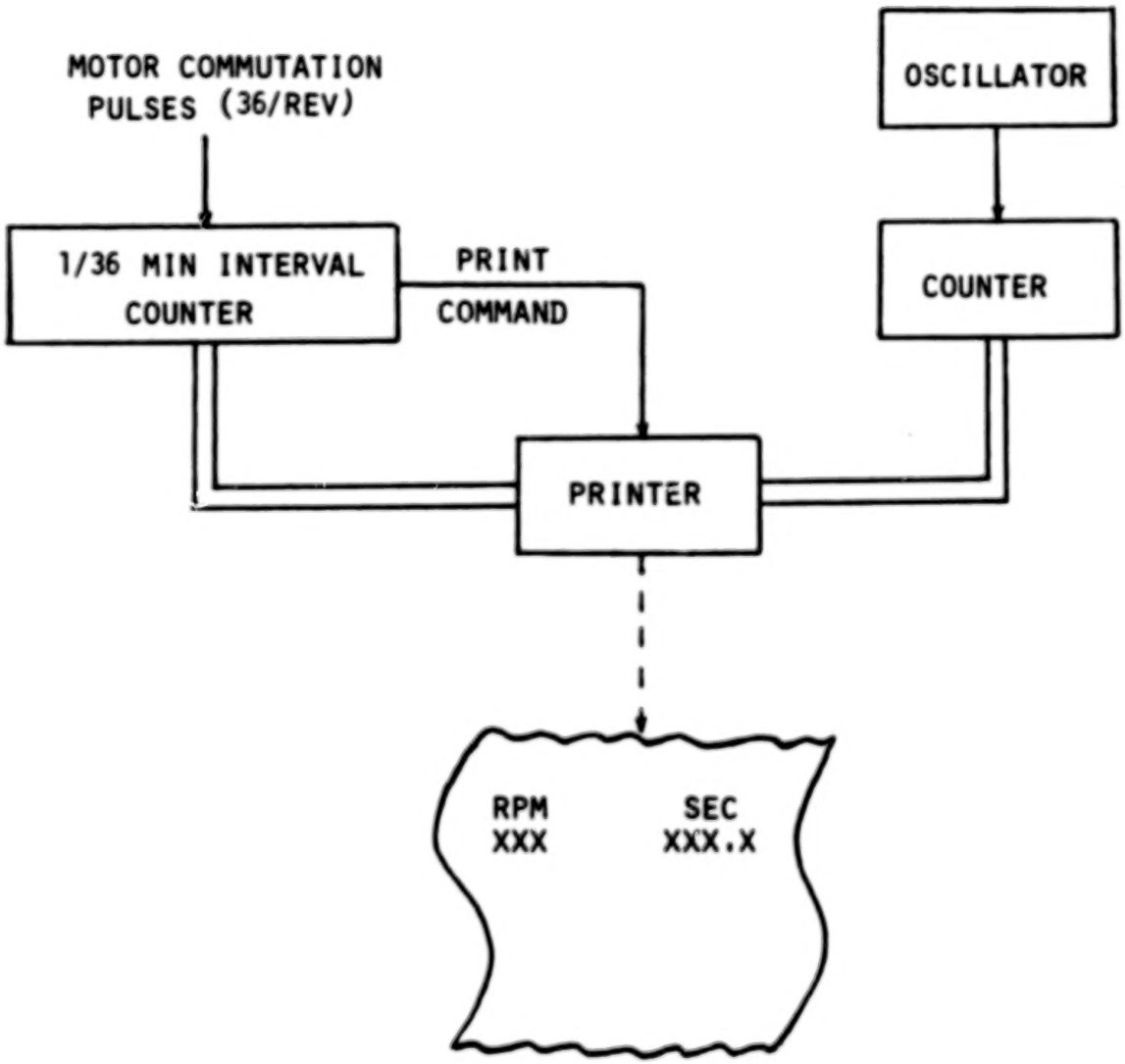

Figure 11.- Data acquisition system used in spin-up and spin-down tests.

1. Report No.	2. Government Accession No.	3. Recipient's Catalog No.
NASA TP-1142		

4. Title and Subtitle	5. Report Date
EVALUATION OF A LABORATORY TEST MODEL ANNULAR MOMENTUM CONTROL DEVICE	March 1978
	6. Performing Organization Code

7. Author(s)	8. Performing Organization Report No.
Nelson J. Groom and David E. Terray	L-11968
	10. Work Unit No. 506-19-13-01
9. Performing Organization Name and Address NASA Langley Research Center Hampton, VA 23665	11. Contract or Grant No.
	13. Type of Report and Period Covered Technical Paper
12. Sponsoring Agency Name and Address National Aeronautics and Space Administration Washington, DC 20546	14. Sponsoring Agency Code

15. Supplementary Notes

16. Abstract

A 4068 N-m-sec (3000 lb-ft-sec) laboratory test model annular momentum control device (AMCD) is described and static and dynamic test results are presented. An AMCD is a spinning annular rim suspended by noncontacting magnetic bearings and powered by a noncontacting linear electromagnetic motor. Test results include spin-motor torque characteristics and spin-motor and magnetic-bearing drag losses. Limitations of some of the design approaches taken are also discussed.

17. Key Words (Suggested by Author(s))	18. Distribution Statement
Spacecraft control actuator Momentum storage device Magnetic suspension	Unclassified - Unlimited Subject Category 31

19. Security Classif. (of this report)	20. Security Classif. (of this page)	21. No. of Pages	22. Price*
Unclassified	Unclassified	22	$4.00

* For sale by the National Technical Information Service, Springfield, Virginia 22161

NASA-Langley, 1978